IEEE Access
Multidisciplinary ⋮ Rapid Review ⋮ Open Access Journal

Received July 22, 2020, accepted July 31, 2020, date of publication August 7, 2020, date of current version August 25, 2020.

Digital Object Identifier 10.1109/ACCESS.2020.3015101

Robust Intelligent Self-Tuning Active Force Control of a Quadrotor With Improved Body Jerk Performance

SHERIF I. ABDELMAKSOUD[1], MUSA MAILAH[1], (Senior Member, IEEE), AND AYMAN M. ABDALLAH[2]

[1]School of Mechanical Engineering, Universiti Teknologi Malaysia, Johor Bahru 81310, Malaysia
[2]Aerospace Engineering Department, King Fahd University of Petroleum and Minerals, Dhahran 31261, Saudi Arabia

Corresponding author: Sherif I. Abdelmaksoud (iasherif@graduate.utm.my)

ABSTRACT This work presents an innovative hybrid control scheme for a quadrotor unmanned aerial vehicle (UAV) model to improve the disturbances rejection capability and body jerk performance by utilizing an active force control (AFC)-based robust intelligent control system via a simulation study. The proposed intelligent control approach incorporates a proportional-integral-derivative (PID) and an intelligent active force control (IAFC) element yielding a robust PID-IAFC scheme. A detailed mathematical model of a quadrotor system with six degrees of freedom (DOFs) was first derived using the *Newton-Euler* method taking into consideration the gyroscopic terms, disturbances, aerodynamics, and friction effects. In the derived model, the PID controller was first designed to stabilize the quadrotor model and achieve the required altitude and attitude motions. In addition, different types of external disturbances in the form of sinusoidal waves and repeated impulses (pulsating) were added. An AFC strategy, known as PID-AFC, was designed and incorporated into the PID controller, and was initially tuned heuristically. Then, an artificial intelligence (AI)-based method employing an iterative learning (IL) algorithm was designed and implemented into the AFC (ILAFC) to estimate the control parameters automatically while on-line. Thereafter, the performance of the ILAFC was compared to the AFC with fuzzy logic (FL) which became known as FLAFC. Also, a self-tuning (ST) PID controller was designed and employed based on the FL method to automatically tune the PID gains based on the prescribed operating and loading conditions. Moreover, a comparative study of the system performance was carried out utilizing the PID, PID-AFC, ILAFC, FLAFC, and ST-FPID-AFC schemes to analyze the system characteristics. Furthermore, the effectiveness of the AFC-based intelligent controller was investigated in connection with the body jerk performance in the presence of external disturbances. The simulated results reveal the effectiveness and robustness of the proposed control strategy based on the IAFC technique in improving the disturbance rejection capability and body jerk performance by 17% in the presence of uncertainties and external disturbances.

INDEX TERMS Quadrotor UAV, active force control, intelligent control, self-tuning, iterative learning, fuzzy logic, robust, body jerk performance.

I. INTRODUCTION

In recent decades, researchers and scientists from diverse sectors have given a great deal of attention to the development of the UAV industry. This is not surprising due to the large number of applications that benefit from using UAVs because of their desirable features including their small size and weight, high maneuverability, low cost, and high degree of automatic stability. They have been used in wide-ranging applications including contour mapping (or profiling of various surfaces/terrains) and traffic monitoring, surveillance, aerial photography and video recording, search and rescue, meteorological reconnaissance, and other civil and military tasks.

Rotary-wing aircraft or rotorcraft systems are a class of UAVs and are distinguished by their ability to vertically take-off and land (VTOL), in addition to hovering in restricted zones. There are various types of rotorcraft

The associate editor coordinating the review of this manuscript and approving it for publication was Xiaosong Hu.

including helicopters, quadrotors, hexacopters, and octocopters [1]. Among these, quadrotors have attracted the attention of a large number of researchers in recent years due to their high maneuverability, VTOL, small size and weight, low cost, reduced maintenance time, and their hovering capability. Despite the tremendous development in quadrotor technology, it still faces certain constraints and impediments, such as limited speed and endurance, high energy consumption, limited power supply (battery), sensitivity to external disturbances, and the restriction to using electrical motors [2].

A quadrotor is a multi-rotor UAV that is lifted by four rotors. It consists of a rigid body connected to four propellers with fixed-pitch blades and airflows that point down to generate an upward-lifting force. The propellers' axes of rotation are fixed and parallel to each other. It has two pairs of identical propellers; two clockwise (CW) and two counter-clockwise (CCW), allowing it to be controlled by varying the speed of the rotors. The quadrotor has six DOFs and only four propellers (inputs) which make it an under-actuated mechanical system with a degree of under-actuation of two [2].

Among the various challenges, tracking the desired trajectories while rejecting various forms of disturbances is essential for quadrotor UAVs to achieve high levels of performance and execution in different operating and loading conditions. For disturbance rejection, several research works have been conducted. One promising strategy is an active disturbance rejection control [3], [4]. Najm and Ibraheem [5] also presented an improved ADRC approach consisting of an improved tracking differentiator (ITD), a linear extended state observer (LESO), and a nonlinear PID controller (NLPID) to stabilize a multirotor model and efficiently expel the exogenous disturbances and uncertainties. The results showed the superiority of the proposed control structure when compared to the conventional PID. Additionally, Dong *et al.* [6] developed, systematically and experimentally, a flight controller utilizing a modified active disturbance rejection method containing a time-optimal tracking differentiator, an extended state observer, and a PD controller for a quadrotor UAV model which could endure streamlined unsettling influences, noises, and input delays.

In relation to trajectory tracking in the presence of wind disturbances, the higher derivatives of motion are rarely discussed. While tracking a certain path, the quadrotor encounters not only the acceleration but also the jerk and higher derivative kinematics. Indeed, acceleration does not begin suddenly, it extends from zero to a certain state, and consequently, some elements of jerkings prevail. In general, designers are trying to reduce the exposure to unnecessary or undesirable motion in order to avoid vibrational levels which may cause failure in the dynamic systems. Thus, reducing the body jerk is deemed to be an important concern [7]. Some research studies have suggested generating optimal trajectories or optimal motion planning frameworks to minimize the body jerk, including the work done by [8]–[10].

One innovative method related to the control of dynamical systems is the active force control (AFC) strategy first demonstrated by Hewit and Burdess in the early eighties [11]. The AFC strategy can typically be integrated with the classical, modern, or intelligent control systems to effectively reject external disturbances [12]. The basic idea of the AFC is to acquire the appropriate estimation of the inertia or mass parameters of the dynamical system by utilizing a crude approximation method [13] or by using any AI approach [12], along with the measurements of the acceleration and force/torque signals generated by the system. A research work is reported in [13] that utilized an AFC-based control scheme to control a quadrotor model. The proposed control system combined a PID controller with the AFC which was tuned by a trial-and-error method (TEM) for controlling only the altitude and yaw motions. The results showed that the PID-AFC strategy significantly improved the altitude control with a much faster response than a conventional PID controller.

In this article, the main contribution of this work is to propose and implement a new hybrid control structure based on an IAFC strategy to stabilize the rotorcraft system, reject the undesired disturbances and improve the body jerk performance effectively and robustly during trajectory tracking. Based on literature, various control strategies have been proposed to reject the external disturbances during trajectory tracking of the quadrotor but the novelty of this work is in suggesting the AFC-based controller for its ease of implementation, simplicity, and robustness, along with its ability to merge seamlessly with intelligent control systems. Moreover, there has been very little research conducted into the utilization of an IAFC based controller for a quadrotor system. The classic PID-AFC tuned by using only a TEM is the most common approach. In addition, this has not been applied to all DOFs of the quadrotor, but limited to only one or two DOFs. Furthermore, no research has yet been conducted into investigating the utilization of an IAFC based control scheme and its effectiveness on the body jerk performance.

The rest of the paper is organized as follows: Section 2 describes the kinematics and dynamics of a quadrotor under certain assumptions. The PID controller and suggested AFC technique with ILC and FLC implementation are presented in Section 3. Section 4 shows the simulation results for the trajectory tracking test based on specific prescribed operating and loading conditions and then goes on to discuss the controller robustness performance. Finally, the paper's conclusion is presented in Section 5.

II. SYSTEM MODELING

The quadrotor is a non-linear multi-input multi-output (MIMO) dynamic system that has a complex structure with high non-linear terms. Thus, obtaining the mathematical model is considered to be a difficult task [1], [2], [14]. In this section, the detailed mathematical model for a quadrotor

is derived, considering the gyroscopic factors, disturbances, aerodynamics, and friction effects.

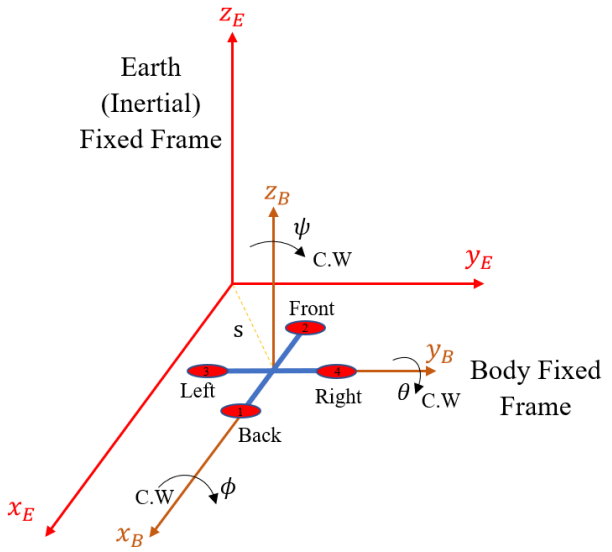

FIGURE 1. The earth (inertial) and body-fixed frames.

A. COORDINATE FRAMES

In order to derive the dynamics of the quadrotor, the coordinate frames used to describe the motion must be initially defined. **Figure 1** shows the earth (inertial) fixed frame, $x_{\mathrm{E}} - y_{\mathrm{E}} - z_{\mathrm{E}}$ and the body-fixed frame, $x_{\mathrm{B}} - y_{\mathrm{B}} - z_{\mathrm{B}}$. The distance between the earth and body-fixed frames is the absolute distance between the center of gravity of each, which is s. The *Euler* angles are utilized for describing the orientation of a model in space with respect to the earth coordinate frame by defining two intermediate coordinate systems, Frame 1 and Frame 2, in addition to the earth and body-fixed frames. Let $R_{\mathrm{E}}^{\mathrm{B}}$ define the rotation from the earth fixed frame to the body-fixed frame. Therefore, the rotation $R_{\mathrm{E}}^{\mathrm{B}}$ is given by:

$$R_{\mathrm{E}}^{\mathrm{B}} = R_{\mathrm{f_2}}^{\mathrm{B}} R_{\mathrm{f_1}}^{\mathrm{f_2}} R_{\mathrm{E}}^{\mathrm{f_1}} \tag{1}$$

where $R_{\mathrm{E}}^{\mathrm{f_1}}$ indicates a rotation from earth Frame E to Frame 1 which is the first intermediate frame, and $R_{\mathrm{f_1}}^{\mathrm{f_2}}$ indicates rotation from Frame 1 to Frame 2 (second intermediate frame) wherein, $R_{\mathrm{f_2}}^{\mathrm{B}}$ describes a transformation from Frame 2 to body Frame B. Therefore, the complete rotation matrix from the body-fixed frame to the earth fixed frame $R_{\mathrm{B}}^{\mathrm{E}}$ is given by:

$$R = R_{\mathrm{B}}^{\mathrm{E}} = \begin{bmatrix} \mathrm{c}\theta\mathrm{c}\psi & \mathrm{s}\phi\mathrm{s}\theta\mathrm{c}\psi - \mathrm{c}\phi\mathrm{s}\psi & \mathrm{c}\phi\mathrm{s}\theta\mathrm{c}\psi + \mathrm{s}\phi\mathrm{s}\psi \\ \mathrm{c}\theta\mathrm{s}\psi & \mathrm{s}\phi\mathrm{s}\theta\mathrm{s}\psi + \mathrm{c}\phi\mathrm{c}\psi & \mathrm{c}\phi\mathrm{s}\theta\mathrm{s}\psi - \mathrm{s}\phi\mathrm{c}\psi \\ -\mathrm{s}\theta & \mathrm{s}\phi\mathrm{c}\theta & \mathrm{c}\phi\mathrm{c}\theta \end{bmatrix} \tag{2}$$

Note that in equation (2) and the others that follow, c = cos and s = sin.

A quadrotor can be considered as five inflexible bodies that are associated together in relative motion [2]. These five

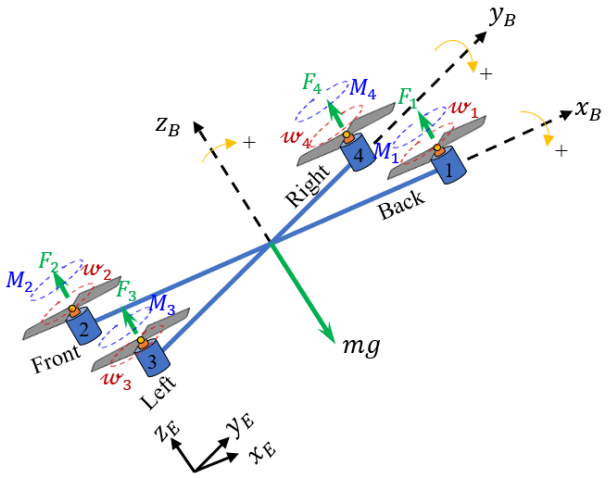

FIGURE 2. Thrust, moment, and rotational speed of each rotor in quadrotor.

bodies are the quadrotor body itself and four propellers attached to the rigid body, as shown in **Figure 2**.

Let $Fr_{\mathrm{E}} : \{O_{\mathrm{E}}, x_{\mathrm{E}}, y_{\mathrm{E}}, z_{\mathrm{E}}\}$ be the earth fixed frame attached to its center of gravity O_{E} and $Fr_{\mathrm{B}} : \{O_{\mathrm{B}}, x_{\mathrm{B}}, y_{\mathrm{B}}, z_{\mathrm{B}}\}$ be the body-fixed frame attached to its center of gravity O_{B}. Also, the rotors' frames are taken to be parallel to each other and attached to their centers of gravity $O_{\mathrm{r_i}}$, and are given by $Fr_{\mathrm{r_i}} : \left\{O_{\mathrm{r_i}}, x_{\mathrm{r_i}}, y_{\mathrm{r_i}}, z_{\mathrm{r_i}}\right\}, i = 1, \ldots, 4$. Also, they are parallel to the body-fixed frame.

In this study, the dynamics of the quadrotor model were obtained based on the *Newton-Euler* method because it is more suitable for modeling based control and it is more convenient to write the equations of motion for each body individually and solve them numerically.

B. SIMPLIFICATION ASSUMPTION

The quadrotor model was derived based on the following assumptions [15]:

- The quadrotor model is rigid and symmetrical.
- The center of gravity of the quadrotor model coincides with the body-fixed frame origin.
- The propellers of the rotor are inflexible (no blade flapping).
- Thrust and drag are proportional to the square of the propeller's speed.
- The axes of the quadrotor coincide with the axes of the body-fixed frame.

The quadrotor is a six DOF system with two sub-systems: the translational sub-system that describes its position (x, y, z) and the rotational sub-system which defines its orientation (ϕ, θ, ψ). The conventional quadrotor model is considered to be an under-actuated system because it has four independent control inputs used to control six DOF motions. In the quadrotor, the rotational sub-system is fully actuated while the translation sub-system is under-actuated. Consider that a quadrotor is represented by a concentrated mass m. Based on

Newton's second law, the translation motions of the quadrotor described in the body frame are obtained by considering its forces described in the earth frame as:

$$F^{\mathrm{E}} = m\frac{d}{dt}(V^{\mathrm{E}}) \tag{3}$$

It is more practical to express equation (3) in the body-fixed frame. In order to achieve that, the *Coriolis* equation is used in which it relates the vector derivatives at two distinctive frames through an angular velocity vector, ω that describes the rotation of the body-fixed frame with respect to the earth fixed frame [16]. Therefore $\sum F^{\mathrm{B}}$ will be as follows:

$$\sum F^{\mathrm{B}} = m\dot{v}^{B} + \omega^{\mathrm{B}} \times (mv^{\mathrm{B}}) \tag{4}$$

where equation (4) is considered as the non-linear translational motion.

For the rotational sub-system, the angular momentum of a body with an inertia matrix, J is described in the earth frame as follows:

$$M^{\mathrm{E}} = J\frac{d}{dt}(\omega^{\mathrm{E}}) \tag{5}$$

Similar to the expression described for the forces in equation (4), the *Euler's* equations may be described in the body-fixed frame to provide the rotational motion. Therefore, $\sum M^{\mathrm{B}}$ will be expressed as follows:

$$\sum M^{\mathrm{B}} = J\dot{\omega}^{\mathrm{B}} + \omega^{\mathrm{B}} \times (J\omega^{\mathrm{B}}) \tag{6}$$

C. DYNAMICS OF QUADROTOR

1) TRANSLATIONAL EQUATIONS OF MOTION

Based on equation (4) and with reference to **Figure 2**, while assuming that the perturbations are small when the quadrotor hovers at a lower height, the translation equations of motion based on *Newton's* second law are obtained as follows [17]:

$$\sum F^{\mathrm{B}} = m\dot{v}^{\mathrm{B}} \tag{7}$$

$$m\dot{v}^{\mathrm{B}} = \begin{bmatrix} 0 \\ 0 \\ -mg \end{bmatrix} + RF_{\mathrm{ng}} + D - F_{\mathrm{d}} \tag{8}$$

$$F_{\mathrm{ng}} = \begin{bmatrix} 0 \\ 0 \\ F_1 + F_2 + F_3 + F_4 \end{bmatrix} = \begin{bmatrix} 0 \\ 0 \\ K_{\mathrm{F}}(\omega_1^2 + \omega_2^2 + \omega_3^2 + \omega_4^2) \end{bmatrix} = \begin{bmatrix} 0 \\ 0 \\ U_1 \end{bmatrix} \tag{9}$$

where

- r: distance of the quadrotor from earth frame, $\begin{bmatrix} x & y & z \end{bmatrix}^{\mathrm{T}}$
- m : mass of the quadrotor
- g : gravitational acceleration
- F_{ng} : non-gravitational forces acting on the quadrotor
- F_{d} : drag forces, $\begin{bmatrix} k_1\dot{x} & k_2\dot{y} & k_3\dot{z} \end{bmatrix}^{\mathrm{T}}$; k_1, k_2, and k_3: aerodynamic translational coefficients
- D : disturbances, $\begin{bmatrix} d_1 & d_2 & d_3 \end{bmatrix}^{\mathrm{T}}$
- K_{F} : aerodynamic force coefficient
- U_1 : altitude control input

After rearrangement, the translational equation of motion can be expressed as [18]:

$$\ddot{x} = \frac{U_1}{m}(\mathrm{c}\phi\mathrm{s}\theta\mathrm{c}\psi + \mathrm{s}\phi\mathrm{s}\psi) - k_1\dot{x} + d_1 \tag{10}$$

$$\ddot{y} = \frac{U_1}{m}(\mathrm{c}\phi\mathrm{s}\theta\mathrm{s}\psi - \mathrm{s}\phi\mathrm{c}\psi) - k_2\dot{y} + d_2 \tag{11}$$

$$\ddot{z} = \frac{U_1}{m}(\mathrm{c}\phi\mathrm{c}\theta) - \mathrm{g} - k_3\dot{z} + d_3 \tag{12}$$

It is obvious that the translational sub-system is under-actuated and depends on both the translational and rotational state variables, as shown in **Figure 3**.

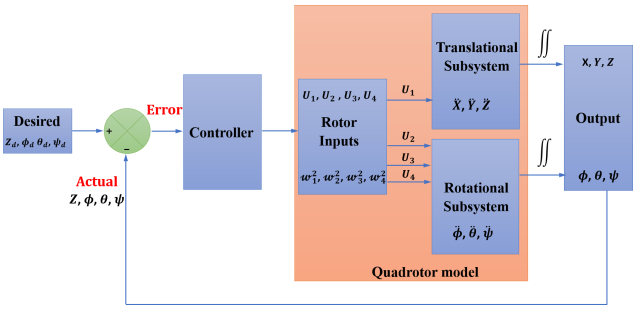

FIGURE 3. Schematic block diagram of a quadrotor UAV.

2) ROTATIONAL EQUATIONS OF MOTION

By using the *Newton-Euler* method, equation (6) can be expressed as [17]:

$$J\dot{\omega} = [M_{\mathrm{Dis}} + M - M_{\mathrm{G}} - M_{\mathrm{Ar}}] - \omega \times J\omega \tag{13}$$

$$F_{\mathrm{i}} = K_{\mathrm{F}}\omega_{\mathrm{i}}^2 \tag{14}$$

$$M_{\mathrm{i}} = K_{\mathrm{M}}\omega_{\mathrm{i}}^2 \tag{15}$$

where

- J : diagonal inertia matrix, $J = \begin{bmatrix} I_{\mathrm{xx}} & 0 & 0 \\ 0 & I_{\mathrm{yy}} & 0 \\ 0 & 0 & I_{\mathrm{zz}} \end{bmatrix}$; I_{xx}, I_{yy}, and I_{zz} are the moments of inertia about the principal axes in the body frame, and the off-diagonal terms are 0 since the quadrotor structure is symmetric.
- ω : angular velocity vector in a body frame, $\omega = \begin{bmatrix} \dot{\phi} \\ \dot{\theta} \\ \dot{\psi} \end{bmatrix}$ and $\dot{\omega} = \begin{bmatrix} \ddot{\phi} \\ \ddot{\theta} \\ \ddot{\psi} \end{bmatrix}$
- M_{Dis} : random disturbance moment
- M : moments acting on the quadrotor in the body frame.
- M_{G} : gyroscopic moments due to the rotors' inertia which is a physical impact in which the moments attempt to adjust the spin axis of the rotor along the z-axis. This can be expressed as:

$$M_{\mathrm{G}} = \omega \times \begin{bmatrix} 0 \\ 0 \\ J_{\mathrm{r}}\omega_{\mathrm{r}} \end{bmatrix} \tag{16}$$

J_{r}: rotors' inertia constant

ϖ_r : rotor relative speed,

$$\varpi_r = \varpi_1 + \varpi_2 - \varpi_3 - \varpi_4$$

- M_{Ar} : friction moment which is the friction of the moving quadrotor body with air
- K_F and K_M: aerodynamic force and moment coefficients, respectively
- ϖ_i : rotational speed of rotor i

Note that ϖ_i is the rotational speed of rotor i, while ω is the angular velocity vector in the body frame and w is the linear velocity in the z_B axis in the body frame.

Each rotor causes an upward force (thrust ($\approx$ lift) F_i) and a moment M_i with the direction opposite to that of the ϖ_i. Propellers 1 and 2 rotate in the same direction (CW) whereas, Propellers 3 and 4 rotate in the opposite direction (CCW) leading to stability in the complete model, balancing the overall torque and canceling the gyroscopic and aerodynamics torques in stationary flight, as depicted in **Figure 2**.

The total moment in x, y, and z directions are given by:

$$M = \begin{bmatrix} lK_F(\varpi_3^2 - \varpi_4^2) \\ lK_F(\varpi_2^2 - \varpi_1^2) \\ K_M(-\varpi_1^2 - \varpi_2^2 + \varpi_3^2 + \varpi_4^2) \end{bmatrix} = \begin{bmatrix} lU_2 \\ lU_3 \\ U_4 \end{bmatrix} \quad (17)$$

where, l is the moment arm, which is the distance between the center of the rotor and the center of gravity of the body frame, while U_2, U_3, and U_4 are the rolling, pitching, and yawing control inputs, respectively.

Therefore, by substitution in equation (13), the rotational equations of motion are given by [18]:

$$\ddot{\phi} = M_{dp} + \frac{lU_2}{I_{xx}} - \frac{\dot{\theta} J_r \varpi_r}{I_{xx}} + \dot{\psi}\dot{\theta}\left(\frac{I_{yy} - I_{zz}}{I_{xx}}\right) - k_4\dot{\phi} \quad (18)$$

$$\ddot{\theta} = M_{dq} + \frac{lU_3}{I_{yy}} + \frac{\dot{\phi} J_r \varpi_r}{I_{yy}} + \dot{\psi}\dot{\phi}\left(\frac{I_{zz} - I_{xx}}{I_{yy}}\right) - k_5\dot{\theta} \quad (19)$$

$$\ddot{\psi} = M_{dr} + \frac{U_4}{I_{zz}} + \dot{\phi}\dot{\theta}\left(\frac{I_{xx} - I_{yy}}{I_{zz}}\right) - k_6\dot{\psi} \quad (20)$$

where

- k_4, k_5, and k_6: aerodynamic friction coefficients
- M_{dp}, M_{dq}, and M_{dr}: random disturbance moments

The relationship between the control laws and the angular speeds of the four rotors, from equations (9) and (17), is given as:

$$\begin{bmatrix} U_1 \\ U_2 \\ U_3 \\ U_4 \end{bmatrix} = \begin{bmatrix} K_F & K_F & K_F & K_F \\ 0 & 0 & K_F & -K_F \\ -K_F & K_F & 0 & 0 \\ -K_M & -K_M & +K_M & +K_M \end{bmatrix} \begin{bmatrix} \varpi_1^2 \\ \varpi_2^2 \\ \varpi_3^2 \\ \varpi_4^2 \end{bmatrix} \quad (21)$$

Thus, to get the angular speeds as a function of the control laws, one has to acquire the inverse of equation (21). It is obvious that the rotational sub-system is fully actuated and depends only on the state variables $x_1 \rightarrow x_6$ that correspond to $[\phi\ \dot{\phi}\ \theta\ \dot{\theta}\ \psi\ \dot{\psi}]$, respectively, as shown in **Figure 3**.

D. BODY JERK

Jerk is a rate of change in the acceleration as a result of a change in the force. From a mathematical point of view, it is the time derivative of the acceleration (a third derivative of the position). The body jerk can be expressed as:

$$\text{Jerk} = \frac{da}{dt} = \frac{d}{dt}(\ddot{x}) = \frac{1}{m}\frac{d}{dt}(F) \quad (22)$$

III. CONTROLLER DESIGN

After the kinematics and dynamics of the quadrotor UAV are derived, a number of control schemes can be designed and experimented with that may eventually lead to an innovative hybrid control scheme that can stabilize the quadrotor, reject the applied disturbances and improve the body jerk performance during trajectory tracking.

A. PROPORTIONAL-INTEGRAL-DERIVATIVE (PID) CONTROLLER

A PID controller is a relatively robust linear controller that is very common in the industry and can be used in a wide range of applications due to its simplicity, practicality, and reliability. The PID family typically comprises the P, PI, PD and PID controllers that include the three gains (controller parameters); the proportional term (K_P) expressing the present error, the integral term (K_I) describing the accumulated past error and the derivative term (K_D) predicting the future error to get the best response. The schematic diagram of the PID controller is shown in **Figure 4**.

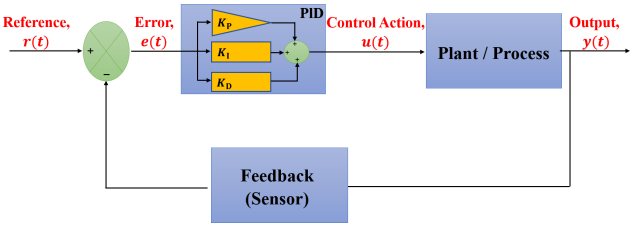

FIGURE 4. Schematic diagram of a PID controller.

The PID controller is not only used for linear systems but can be also applied to non-linear and coupled systems. Many types of research use a standard PID controller for controlling the quadrotor UAV, either practically [19] or analytically [20]. The PID control parameters can be tuned using a trial-and-error method (TEM), a look-up table, optimization methods, or intelligent techniques. One such method is by using the look-up table as in the *Ziegler-Nichols* method [21], while other researchers used a standard PID controller tuned by genetic algorithm (GA) to achieve an improvement in the stability and execution of the system performance [15], [18], [22]. The results showed the

effectiveness and robustness of the PID scheme in trajectory tracking although the PID compensation was deemed ineffective at rejecting external disturbances such as windy environments [22].

To design a PID controller, generally, the following equation is utilized:

$$G(s) = K_{\mathrm{P}} + \frac{K_{\mathrm{I}}}{s} + K_{\mathrm{D}}s \tag{23}$$

Therefore, the output of the PID controller can be expressed as:

$$m(s) = G(s)\,e(s) = K_{\mathrm{P}}e(s) + \frac{K_{\mathrm{I}}e(s)}{s} + K_{\mathrm{D}}se(s) \tag{24}$$

where $e(s)$ is the error:

$$e(s) = \text{Reference} - \text{Output} \tag{25}$$

1) POSITION CONTROL

Based on the dynamics of the translational and rotational subsystems, the altitude and orientation of the quadrotor are controlled based on the control laws U_1, U_2, U_3, and U_4. While the x and y positions cannot be controlled directly by utilizing one of the four control laws they can be controlled using the roll and pitch angles. The calculated ϕ_{d} and θ_{d} have to be limited to a range of between -20° and 20° to fulfill the small-angle assumption and can be expressed as:

$$\phi_{\mathrm{d}} = \frac{m}{U_1}(U_{\mathrm{x}}\mathrm{s}\psi - U_{\mathrm{y}}\mathrm{c}\psi) \tag{26}$$

$$\theta_{\mathrm{d}} = \frac{m}{U_1}(U_{\mathrm{x}}\mathrm{c}\psi + U_{\mathrm{y}}\mathrm{s}\psi) \tag{27}$$

where the closed-loop simulation for the complete quadrotor model has two control loops: an inner loop which contains the altitude and the orientations (Z, ϕ, θ, and ψ) and an outer loop that includes the position (x and y) as shown in **Figure 5**.

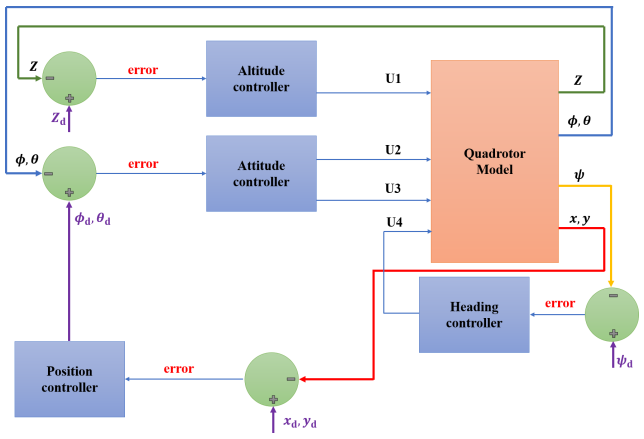

FIGURE 5. Schematic block diagram of a quadrotor UAV.

B. ACTIVE FORCE CONTROL

Active force control (AFC) is an innovative technique based on the classic *Newton's* second law of motion. A schematic diagram of the AFC is shown in **Figure 6**. The main advantage of the AFC technique is its ability to reject any

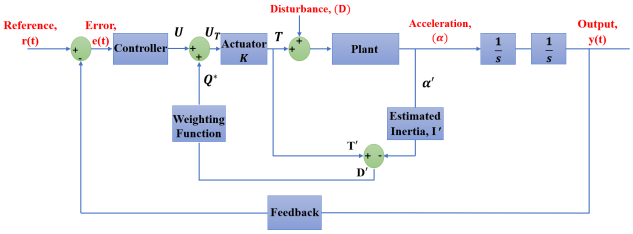

FIGURE 6. Schematic diagram of the AFC technique.

known/unknown and internal/external disturbances in the dynamic system effectively, while keeping the system robust and stable during the system's operation [23]. The AFC strategy is mainly based on the appropriate estimation of the estimated mass or inertia of the system dynamics, the accurate measurement of the force (or torque), and the acceleration of the physical system. The open-loop transfer function (plant) can be obtained by considering the following expression:

$$TF = \frac{\alpha}{T} = \frac{\alpha}{U_{\mathrm{T}}} \tag{28}$$

where

- T : torque applied to the system
- U_{T}: total control output signal
- α : angular acceleration

If external disturbances are applied to the dynamic system:

$$TF = \frac{\alpha}{T + D} \tag{29}$$

Implementing the AFC strategy:

$$TF = \frac{\alpha}{U_{\mathrm{T}} + D} = \frac{\alpha}{U + Q^* + D} \tag{30}$$

where

- D : disturbance applied to the system
- U : control output signal
  $Q^* = WF * D'$
  $D' = T' - I'\alpha'$
- Q^* : AFC output signal
- WF : weighting function
- D': estimated disturbance torque
- T' : measured torque
- I' : estimated mass moment of inertia
- α' : measured angular acceleration

The superscript ($'$) represents the measured, estimated, or computed parameters. T' and α' are measurable quantities that can be measured using a torque sensor and an accelerometer, respectively.

C. ITERATIVE LEARNING CONTROL (ILC)

One innovative intelligent control strategy is ILC, or what is called a betterment process, which is considered to be a type of adaptive intelligent control that acts smartly to enhance the automatic control systems and achieve higher performance levels in reference tracking. This is based on the improvement of the transient response of dynamic systems that operate repetitively over a fixed time interval as proposed by

Arimoto *et al.* [24]. It enhances the system performance by utilizing prior information about the previous iterations [25]. Also, it solves the problem encountered by the system which is subjected to various forms of inputs. A schematic diagram illustrating the IL principle is shown in **Figure 7**.

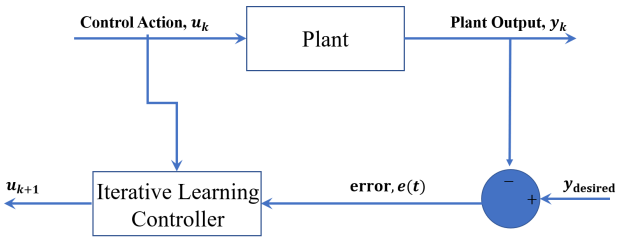

FIGURE 7. Schematic diagram of the ILC technique.

It is important to apply an algorithm for generating the next control input in such a manner that the impact of the error is either reduced or converged on successive trails. Due to the analogous relationship of the mathematical expression to the classical PID control, the IL algorithm could be duly described as a P, PI, PD, or PID-type ILC algorithm [24].

The learning control rule for the PID-type can be expressed mathematically as [24]:

$$u_{k+1}(t) = u_k(t) + Ke_k(t) \tag{31}$$

where

- $u_{k+1}(t)$: next step value of the output
- $u_k(t)$: current output value
- $e_k(t)$: current error value
- K : designed parameter (constant)

containing the PID term,

$$K = \phi + \Gamma \int dt + \psi \frac{d}{dt}$$

ϕ, Γ, and ψ: learning parameters associated with the P, I and D terms, respectively.

In this study, a PD-type IL algorithm was utilized and embedded into the ILAFC scheme to determine the appropriate value of the estimated inertia automatically, as follows:

$$IN_{k+1} = IN_k + Ke_k(t) \tag{32}$$

where

- IN_{k+1} : next step value of the estimated inertia
- IN_k : current value of the estimated inertia
- $K = \phi + \psi \frac{d}{dt}$

A schematic block diagram of the proposed ILAFC is shown in **Figure 8**. Dong and He applied a novel fuzzy PID-ILC algorithm successfully to the trajectory tracking of a quadrotor UAV [26], while Allahverdy *et al.* proposed a backstepping integral sliding mode control (BISMC) with an ILC algorithm for controlling the translational and rotational dynamics of the quadrotor [27]. For the IL algorithm, a stopping criterion is best defined as halting the learning iteration when it is deemed that learning has successfully achieved the

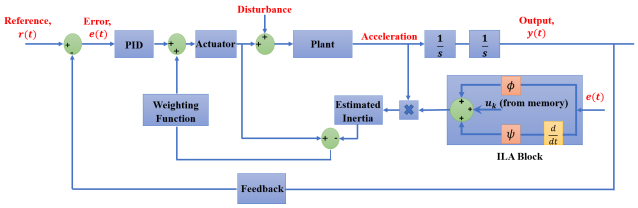

FIGURE 8. A schematic diagram of PID–ILAFC.

iteration count limit or the desired parameter has successfully converged. In this study, the ILC was designed and implemented for tuning the estimated inertia of the AFC strategy, where the stopping criterion was assigned when the error is anticipated to meet a value near the zero datum.

D. FUZZY LOGIC CONTROL (FLC)

FLC is a type of intelligent control method that is either a knowledge-based or a rule-based system. The fuzzy logic concept was first introduced by Lotfi Zadeh in 1965. It utilizes data and intelligent computing to derive the control output. Its principle is based on the fuzziness in the real-world and the simulation of human experience by incorporating the linguistic variables and the IF-THEN rules. The FLC is distinguished among other intelligent methods as using subjective human thinking throughout the controller design to find the solution to the problem. This is very suitable for complex dynamic models, highly non-linear systems, or incomplete information systems without deep theoretical knowledge. For control implementation, there are two main fuzzy implications – the *Mamdani* type rule and the *Takagi-Sugeno* rule. In this study, the *Mamdani* type rule was utilized for designing the FLC as a tuning tool. There are four basic steps to implement FLC; ***Fuzzification*** which converts the crisp value into a fuzzy value, ***Ruled Evaluation*** which produces the output based on certain rules, ***Aggregation*** which combines the consequences of each rule into a single fuzzy set output, and finally ***Defuzzification*** which converts the fuzzy output into a crisp output.

An FLC has been proposed for controlling the quadrotor. Kuantama *et al.* [28] demonstrated modeling and control of a quadcopter system using a standard PID controller and a PID controller tuned by an FLC. It appeared that the fuzzy-PID controller is more compelling and productive in canceling the outside disturbances, reducing the errors, and automatically adjusting the tracking response compared to a standard PID controller [28], [29]. Demir *et al.* [30] further studied, both numerically and experimentally, the attitude control and real-time trajectory tracking of a quadcopter model by utilizing a self-tuning fuzzy PID controller. In this section, FLC was used for self-tuning the PID controller based on the prescribed operation and loading conditions and also for determining the appropriate value of the estimated inertia in the AFC loop. They were employed to control the quadrotor performance and later compared to other schemes based on system characteristics.

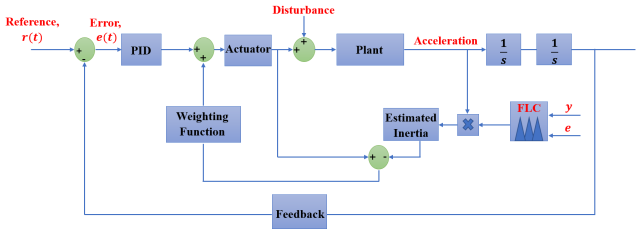

FIGURE 9. A schematic diagram of PID–FLAFC.

1) SELF-TUNING OF THE INERTIA VALUE FOR THE AFC STRATEGY

In this section, the FLC was used for estimating the value of the estimated inertia automatically, as shown in the schematic block diagram of **Figure 9**. In the FLAFC block, there are two inputs - the error $e(t)$ and the actual response $y(t)$, whereas there is only one output which is the estimated inertia value.

The rule-based inferences applied in the FLAFC system were also suggested based on the expert user experiences as shown in **Table 1**. The linguistic variables used for the error, the actual response, and the estimated inertia were all defined as [Small (S), Medium (M), Large (L)]. Meanwhile, the triangular membership function was applied for all of the variables, while the centroid technique was utilized for defuzzification in the *Mamdani* engine.

TABLE 1. Rule-based inferences applied in FLAFC.

		$y(t)$		
		S	M	L
$e(t)$	S	L	L	M
	M	L	M	M
	L	M	M	S

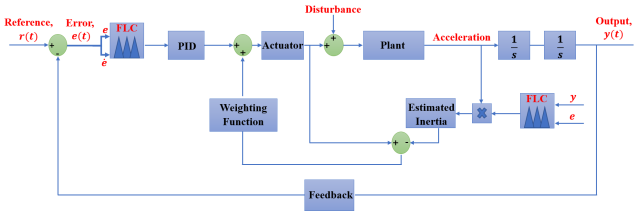

FIGURE 10. A schematic diagram of ST-FPID-AFC.

2) SELF-TUNING FUZZY PID CONTROLLER (ST-FPID)

For the quadrotor model, the PID controller was used as the main control system, whereas the FLC was used to provide the automatic adjustment of the PID controller parameters based on the given loading and operating conditions, as shown in **Figure 10**. The self-tuning fuzzy PID controller was proposed based on work by Zhao (1993). There are two inputs for the ST-FPID scheme comprising the error and the derivative of the error, whereas there are three outputs for the system - K_P, K_D, and α. The error $e(t)$ is the difference between the setpoint and the actual responses, while the derivative of the error $\dot{e}(t)$ is the rate of the error. For the output, K_P is the proportional gain, K_D is the derivative gain, and α is the variable that is utilized to obtain the K_I value and based on equation (22), another equivalent form of the PID control algorithm can be expressed as [31]:

$$G(s) = K_P(1 + \frac{1}{T_i s} + T_d s) \tag{33}$$

where

- T_i : integral time constant $= \frac{K_P}{K_I}$
- T_d : derivative time constant $= \frac{K_D}{K_P}$

The relationship between the derivative and the integral time constants can be expressed as follows:

$$T_i = \alpha T_d \tag{34}$$

By substituting and rearranging the previous equation:

$$K_I = K_P^2 \Big/ \alpha K_D \tag{35}$$

The rule-based inferences applied in the ST-FPID scheme were proposed based on expert user knowledge and experiences and the rule-based inferences of K_P which can be seen in **Table 2**. The linguistic variables used for error and the derivative of error were both defined as [Very Small (VS), Small (S), medium (M), Large (L), Very Large (VL)] while K_P and K_D were characterized as [Big (B) and Small (S)] whereas α was defined as [Very Small (VS), Small (S), medium (M), Large (L), Very Large (VL)]. Meanwhile, the triangular membership function was applied to all variables, while the center of gravity technique was employed for defuzzification in the *Mamdani* engine.

TABLE 2. K_P rule-based inferences applied to the ST-FPID scheme.

		K_P				
		$\dot{e}(t)$				
		VS	S	M	L	VL
$e(t)$	VS	B	B	B	B	B
	S	S	B	B	B	S
	M	S	S	B	S	S
	L	D	B	B	B	S
	VL	B	B	B	B	B

Moreover, regarding the stability analysis of the PID-AFC scheme, it was shown that the stability of the system is independent of the quadrotor model; however, it depends on the actuator dynamics, the PID parameters, and the estimated inertia in the AFC strategy. Thus, the stability of the quadrotor model will not affect the stability of the whole system. Also, this is a guarantee that the system displays responses that are limited when it is excited with proper inputs to the system [32].

IV. SIMULATION, RESULTS, AND DISCUSSION

A. SIMULATION

In this section, the derived dynamic system and the proposed control systems were implemented and simulated using MATLAB/Simulink software, while the *Fuzzy Logic Toolbox* was employed for applying the FLC and the self-tuning fuzzy aspects. A number of control schemes, i.e., the PID, PID-AFC, ILAFC, FLAFC, and ST-FPID-AFC were simulated and numerically experimented with, after which a comparative study was carried out to analyze the performance of system characteristics based on their effectiveness. To assess the control strategies' performance, various operating and loading conditions were considered. Disturbances were added to the quadrotor UAV dynamic system in the form of forces and moments to give the effect of a windy environment. The quadrotor model has been subjected to two different types of disturbances: a sinusoidal wave and a repeated pulse of equal sizes and periods (pulsating disturbances), as shown in **Figure 11**. The amplitude and frequency of the sinusoidal wave were set to 1 m and 1 Hz, respectively, as shown in **Figure 11 (a)**; whereas the amplitude, period, width and delay for the repeated disturbance are 1 m, 2 s, 30 m, and 1 s, respectively, as shown in **Figure 11 (b)**. The controller output signal is directly fed into the derived dynamic model without any mapping in the actuator. The values of the quadrotor parameters are listed in **Table 3**, while the PID controller gains that are tuned heuristically are shown in **Table 4**. The expected results were analyzed in time domain, noting that the objective of the control system parameter tuning is to minimize the peak time, the settling time, and the steady-state error.

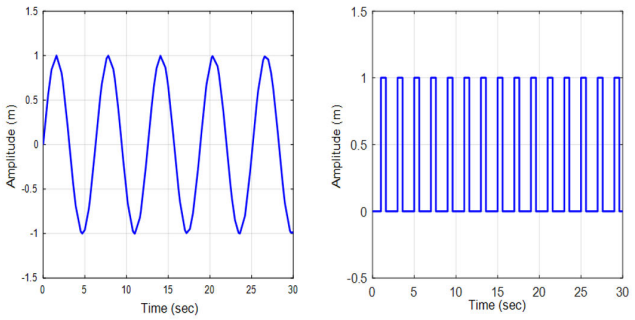

FIGURE 11. (a) Sinusoidal wave and (b) pulsating disturbances.

B. RESULTS AND DISCUSSION

In this section, a comparison study of all of the proposed control systems was conducted in the time domain through simulation, where the simulations of the model were solved using the *ode45* with a variable-step solver and a relative tolerance of 0.001. Two types of disturbances were introduced into the quadrotor system, namely, a sinusoidal wave and pulsating disturbances to check the efficacy of the proposed control schemes in stabilizing the system and rejecting the applied disturbances where they were activated only on the dynamic system. Based on the position control, the dynamic system outputs x, y,z, and ψ were considered to be relevant for the effectiveness of control schemes and the behavior of the quadrotor model. A summary of system performances for all of the control strategies is shown in **Figures 12** and **13**. Also, the system characteristics for all of the cases are demonstrated by utilizing bar charts in **Figures 14** and **15** where TS, TP, and SSE are the settling time, peak time, and steady-state error, respectively. It is evident that all the proposed control schemes have revealed improvements in the system performance compared to their conventional PID counterpart. Also, the suggested AFC-based controllers showed superior execution in damping the vibrational levels, oscillations, and external disturbances.

The results also revealed the inability of the PID controller to expel the external disturbances successfully. Moreover, the results of the simulations showed the robustness and the effectiveness of the PID-AFC tuned by a crude approximation method in stabilizing the quadrotor system while

TABLE 3. Quadrotor system parameters [17], [33].

Description	Unit	Value
Quadrotor mass, m	kg	0.65
Distance from the center of mass to each motor, ℓ	m	0.23
Moment of inertia about the x-axis, I_{xx}	kgm^2	7.5E-3
Moment of inertia about the y-axis, I_{yy}	kgm^2	7.5E-3
Moment of inertia about the z-axis, I_{zz}	kgm^2	1.3E-2
Gravity, g	m/s^2	9.8
Thrust force coefficient, K_F	Ns^2	3.13E-5
Moment coefficient, K_M	mms^2	7.5E-7
Moment of inertia of the rotor, J_r	kgm^2	6E-5
Translational drag force coefficients, K_1, K_2, K_3	Ns/m	0.01
Aerodynamic friction, K_4, K_5, K_6	Ns/rad	0.012
Attitude's saturation	$20° \geq \phi, \theta, \psi \geq -20°$	

TABLE 4. PID controller parameters for various types of motion using a heuristic method.

	Motion					
Gains	x	y	z	ϕ	θ	ψ
K_P	5	5	10	0.5	0.5	0.1
K_I	0	0	4	0	0	0
K_D	1	1	5	0.5	0.5	0.1

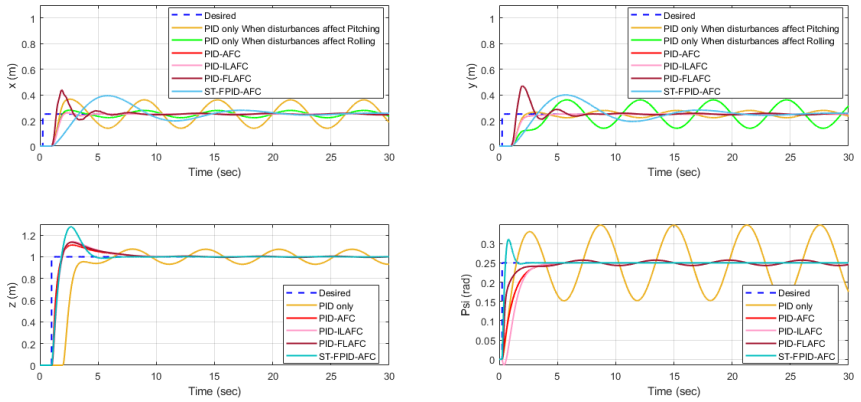

FIGURE 12. Time response of all the control schemes in the presence of the sinusoidal wave disturbance.

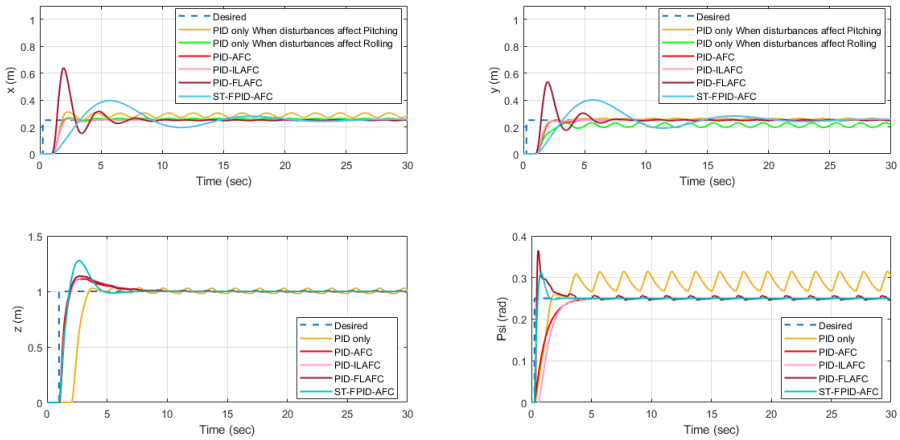

FIGURE 13. Time response of all the control schemes in the presence of pulsating disturbance.

efficiently rejecting the disturbances. Also, the simulated results revealed the high coupling impact for the forward and sideward motions, and the rolling and pitching motions. Furthermore, it is observed that, when the disturbances result in a rolling movement (which in turn causes a sideward motion along the *y*-axis), it also affects the forward motion and vice versa.

It is thus evident that the AFC based controller is capable of stabilizing these effects and simultaneously rejecting the external disturbances. It is also important to note that the computed value of the estimated inertia in the AFC strategy is considered to be crucial for effective AFC implementation.

The AI methods using IL and FL were later introduced for automatically determining on-line, the appropriate value of the estimated inertia in the AFC loop. The results showed the robustness and effectiveness of the ILAFC scheme in stabilizing the quadrotor system and expelling the introduced disturbances efficiently. The importance of the ILAFC is in its ease of design, efficiency, and automatic tuning. Moreover, for real-time implementation, the ILAFC is considered as an effective control scheme because of its ability to automatically adjust the control parameters on-line in contrast to some of the other control systems that need to adjust their control parameters off-line. Regarding the comparison between the ILAFC and FLAFC, the results imply that the ILAFC shows better performance than the FL for the quadrotor based on the responses and the characteristics of the system. However, one of the exceptional benefits of using FL is that it does not require any precise mathematical formulation or model; the user experience and judgment is typically the only pre-requisite.

With regard to ST-FPID-AFC, the results exhibit the impressive ability of the proposed strategy to stabilize the quadrotor model and reject the unsettling outside influences. In comparison to the previous control schemes, the ST-FPID-AFC scheme is considered to be one of the best options among the other proposed control systems involving no prior knowledge of the control system parameters or the dynamic system, various loading and operating conditions, and unknown disturbances. In these previous cases, the PID controller parameters were tuned using the heuristic method. This needs many trials and is time-consuming to obtain the appropriate gain values, unlike the FPID controller that can adjust its parameters effectively based on the surrounding environment and conditions.

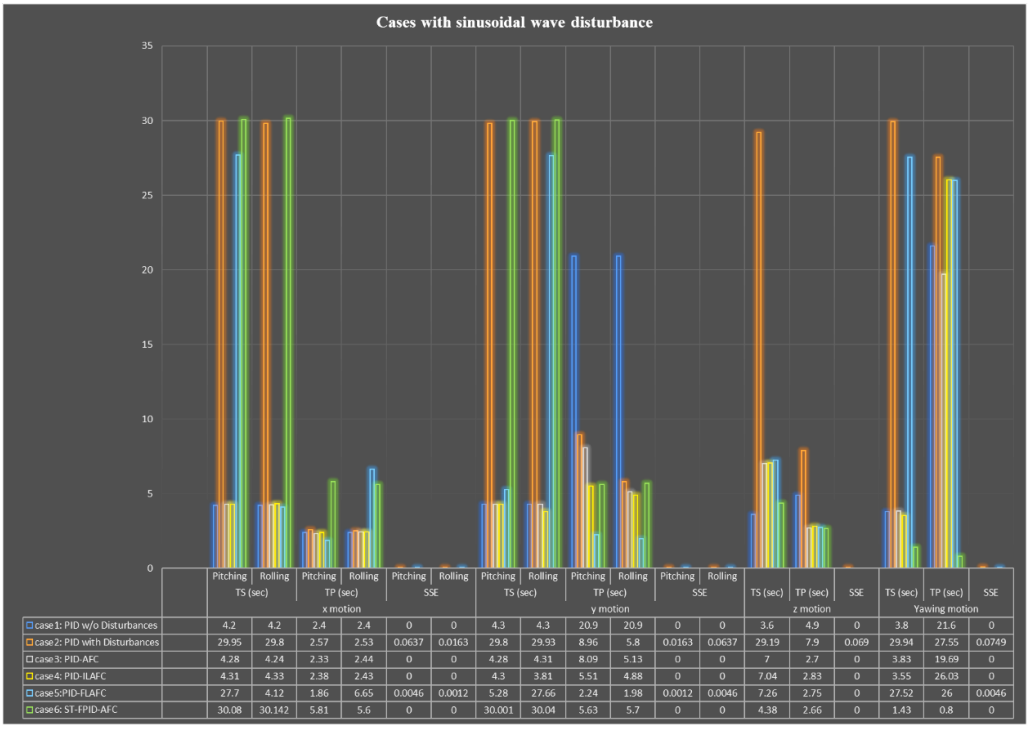

	Pitching TS (sec)	Rolling TS (sec)	Pitching TP (sec)	Rolling TP (sec)	Pitching SSE	Rolling SSE	Pitching TS (sec)	Rolling TS (sec)	Pitching TP (sec)	Rolling TP (sec)	Pitching SSE	Rolling SSE	TS (sec)	TP (sec)	SSE	TS (sec)	TP (sec)	SSE
	x motion						y motion						z motion			Yawing motion		
case1: PID w/o Disturbances	4.2	4.2	2.4	2.4	0	0	4.3	4.3	20.9	20.9	0	0	3.6	4.9	0	3.8	21.6	0
case2: PID with Disturbances	29.95	29.8	2.57	2.53	0.0637	0.0163	29.8	29.93	8.96	5.8	0.0163	0.0637	29.19	7.9	0.069	29.94	27.55	0.0749
case3: PID-AFC	4.28	4.24	2.33	2.44	0	0	4.28	4.31	8.09	5.13	0	0	7	2.7	0	3.83	19.69	0
case4: PID-ILAFC	4.31	4.33	2.38	2.43	0	0	4.3	3.81	5.51	4.88	0	0	7.04	2.83	0	3.55	26.03	0
case5:PID-FLAFC	27.7	4.12	1.86	6.65	0.0046	0.0012	5.28	27.66	2.24	1.98	0.0012	0.0046	7.26	2.75	0	27.52	26	0.0046
case6: ST-FPID-AFC	30.08	30.142	5.81	5.6	0	0	30.001	30.04	5.63	5.7	0	0	4.38	2.66	0	1.43	0.8	0

FIGURE 14. Characteristics of the suggested control schemes for the sinusoidal wave disturbance.

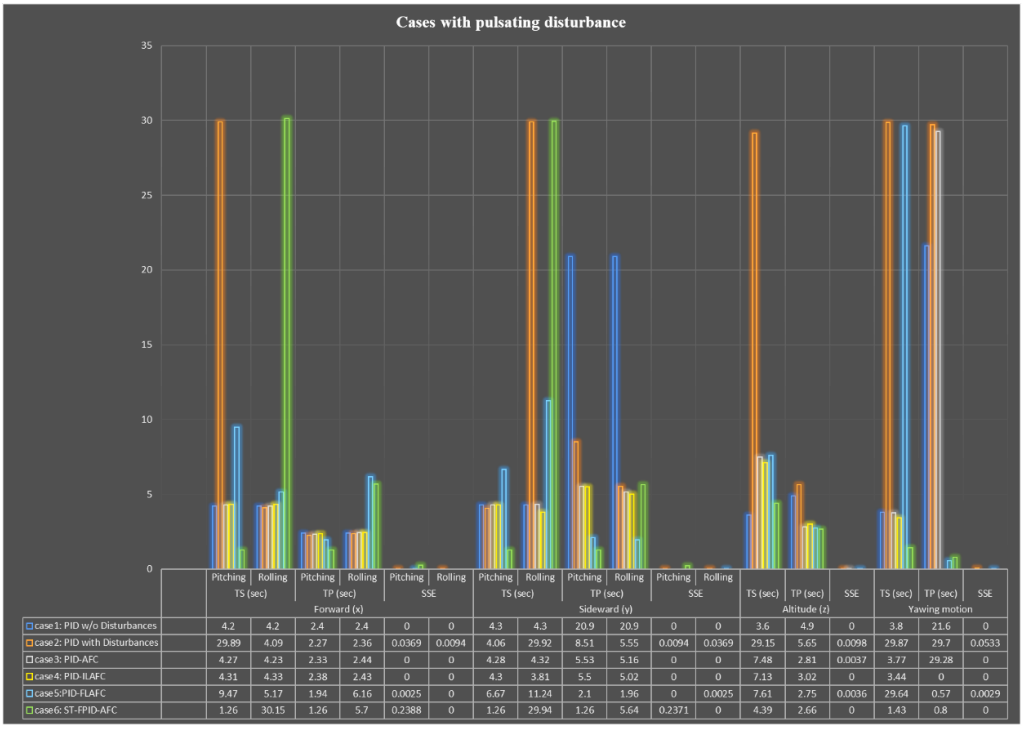

	Pitching TS (sec)	Rolling TS (sec)	Pitching TP (sec)	Rolling TP (sec)	Pitching SSE	Rolling SSE	Pitching TS (sec)	Rolling TS (sec)	Pitching TP (sec)	Rolling TP (sec)	Pitching SSE	Rolling SSE	TS (sec)	TP (sec)	SSE	TS (sec)	TP (sec)	SSE
	Forward (x)						Sideward (y)						Altitude (z)			Yawing motion		
case1: PID w/o Disturbances	4.2	4.2	2.4	2.4	0	0	4.3	4.3	20.9	20.9	0	0	3.6	4.9	0	3.8	21.6	0
case2: PID with Disturbances	29.89	4.09	2.27	2.36	0.0369	0.0094	4.06	29.92	8.51	5.55	0.0094	0.0369	29.15	5.65	0.0098	29.87	29.7	0.0533
case3: PID-AFC	4.27	4.23	2.33	2.44	0	0	4.28	4.32	5.53	5.16	0	0	7.48	2.81	0.0037	3.77	29.28	0
case4: PID-ILAFC	4.31	4.33	2.38	2.43	0	0	4.3	3.81	5.5	5.02	0	0	7.13	3.02	0	3.44	0	0
case5:PID-FLAFC	9.47	5.17	1.94	6.16	0.0025	0	6.67	11.24	2.1	1.96	0	0.0025	7.61	2.75	0.0036	29.64	0.57	0.0029
case6: ST-FPID-AFC	1.26	30.15	1.26	5.7	0.2388	0	1.26	29.94	1.26	5.64	0.2371	0	4.39	2.66	0	1.43	0.8	0

FIGURE 15. Characteristics of the suggested control schemes for pulsating disturbance.

In this study, the effectiveness of utilizing the AFC-based controller on the body jerk performance in the presence of external disturbances is also investigated. Amongst the proposed control schemes, the PID-ILAFC strategy was used to test its robustness for the body jerk performance. Here, the sinusoidal wave and pulsating disturbances were applied as external disturbances and in the z-direction only. Three cases were studied in relation to the body jerk performance, with reference to equation (22): PID without any disturbances, PID with external disturbances, and

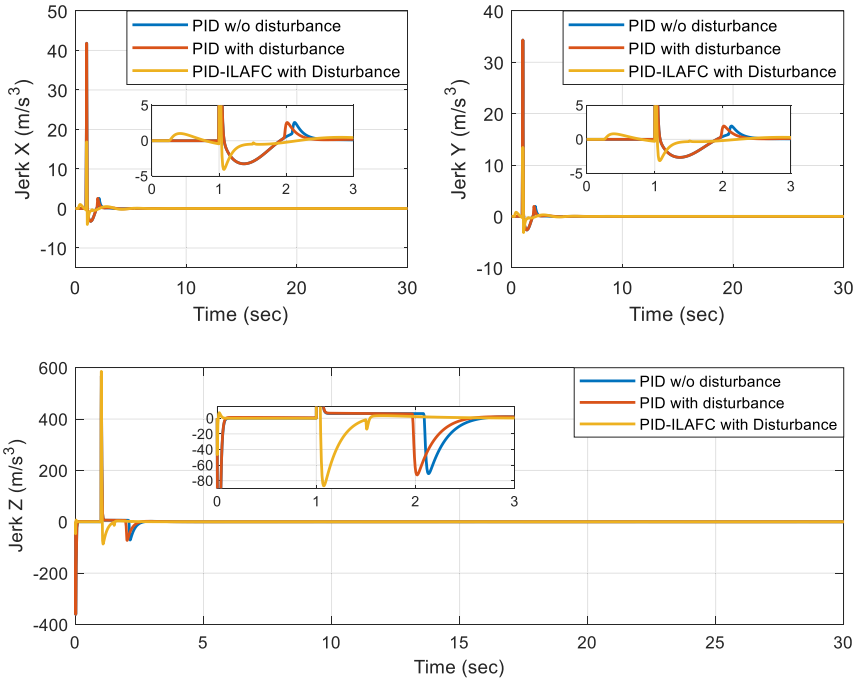

FIGURE 16. Responses of the body jerk performance in the presence of sinusoidal wave disturbance.

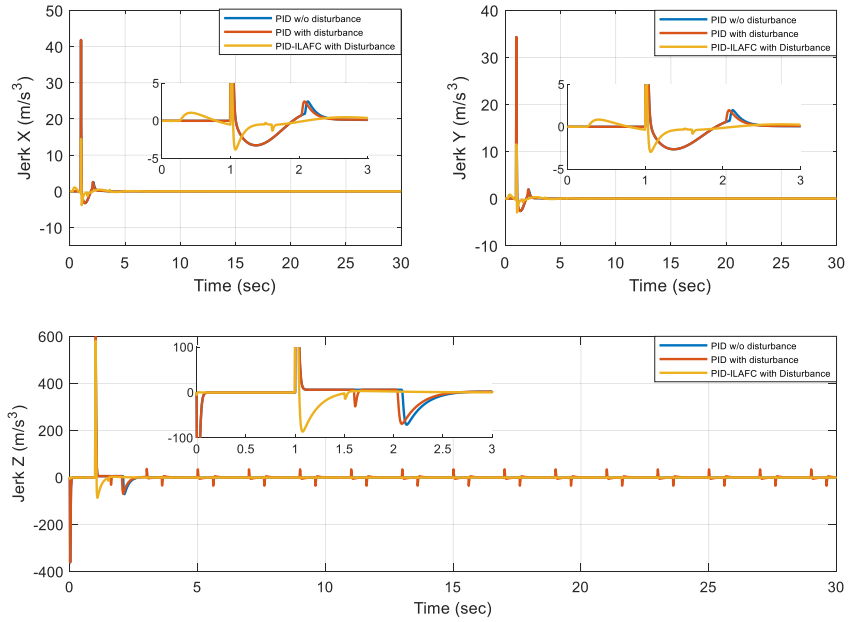

FIGURE 17. Responses of the body jerk performance in the presence of pulsating disturbance.

PID-ILAFC with external disturbances. The responses of the body jerk performance for these three schemes are presented in **Figures 16** and **17**. Here, the root mean square (RMS) level was used to deduce the best result and can be expressed as:

$$\mathrm{RMS} = \sqrt{\frac{1}{N}\sum_{i=1}^{N}[x_i]^2} \tag{36}$$

where N is the sample size and x is the output signal.

The RMS level values of the cases' responses are listed in **Tables 5** and **6**. To assess the body jerk performance, the percentage of the root mean square error (RMSE) was calculated where the PID system was considered as the basis for comparison for acquiring the improvement percentage.

From **Figures 16** and **17**, the simulated results revealed the ability of the IAFC based controller in improving the body jerk performance. From **Tables 5** and **6**, the percentages of the improvement in the body jerk performance for x,y, and z motions, are 59%, 60%, and 17%,

TABLE 5. Characteristics of the quadrotor dynamics with sinusoidal wave disturbance.

	Motion	RMSE
PID without Disturbances	x	1.12
	y	0.92
	z	17.37
PID with Disturbances	x	1.12
	y	0.92
	z	17.4
PID-ILAFC with Disturbances	x	0.46
	y	0.36
	z	14.45

TABLE 6. Characteristics of the quadrotor dynamics with pulsating disturbance.

	Motion	RMSE
PID without Disturbances	x	1.12
	y	0.92
	z	17.37
PID with Disturbances	x	1.12
	y	0.92
	z	18.6
PID-ILAFC with Disturbances	x	0.41
	y	0.32
	z	14.3

respectively and the sinusoidal wave disturbance, 63%, 65%, and 18%, respectively. For pulsating disturbances, where the RMSE decreases, the body jerk performance becomes better. Even the body jerk showed some oscillations when utilizing PID-ILAFC, however, the overall performance is far better than for PID only, in the presence of external disturbances.

The findings serve to provide more insights into the field of rotorcraft systems in the areas of disturbance rejection and effective control capability during trajectory tracking. Thus, it can be summarized that the hybrid control schemes based on the IAFC strategy for the quadrotor model, as an example of rotorcraft UAVs, are robust against various forms of disturbances and uncertainties, while at the same time achieving the desired system stability with minimal tracking error. Besides, the proposed control strategies are able to effectively reject disturbances without the need to increase the torque of the actuator or retuning the PID controller gains and it is proven that the proposed control systems can guarantee that all the closed-loop signals are efficiently tracking the reference trajectories. On top of that, the IAFC-based control systems are able to efficiently improve the body jerk performance by at least 17% in the presence of uncertainties and external disturbances and reduce the exposure to unnecessary or undesirable motions to avoid vibrations and oscillations that may cause failure in the aerial systems.

It is worth reiterating here that this work is yet another robust AFC-based scheme applied to a more sophisticated aerial system considering more challenging operating and loading conditions to enhance the disturbance rejection capability and control improvement, especially in the body jerk performance.

By applying the proposed IAFC-based controller to the 6-DOF quadrotor system, it can be seen that it is characterized by its ease of implementation and low computational burden due to the use of relatively simple control algorithms, particularly those related to PID, AFC and ILC. This in turn implies a huge potential implication for real-time implementation. Arguably, the main constraints in the implementation of the AFC strategy are the limited actuator's bandwidth that restricts the AFC output signal and the presence of the algebraic loop that can be solved by adding a delay within the model.

V. CONCLUSION

The external disturbances and windy environment are considered to be challenges that face the quadrotor UAVs during trajectory tracking. The quadrotor being a highly nonlinear, under-actuated, and complex dynamical system was rigorously analyzed taking into account the gyroscopic terms, external disturbances, aerodynamics, and friction impacts. The proposed PID-AFC, PID-ILAFC, PID-FLAFC, and ST-FPID-AFC schemes have been successfully designed and implemented to analyze the system behavior and characteristics. The AFC-based schemes clearly showed robust performance in stabilizing the quadrotor model and in rejecting different types of the introduced disturbances, i.e., the sinusoidal wave and pulsating disturbances when compared to the conventional PID controller counterpart. Furthermore, the IAFC based hybrid novel control structure showed a notable 17% improvement in body jerk performance in the presence of uncertainties and external disturbances. Future works should focus on validating the practical and real-time implementation of the proposed PID-IAFC strategy on a physical quadrotor UAV model. It will be very useful to further evaluate the practical viability of the method for using the proposed controller in a real-world scenario, considering various real operating and loading conditions. The IAFC-based controller can also be particularly applied to explore its ability to suppress the swing load vibrations of a quadrotor-slung load system for transportation mission. Further research might consider the actuator mapping with the proposed control schemes.

REFERENCES

[1] S. N. Ghazbi, Y. Aghli, M. Alimohammadi, and A. A. Akbari, "Quadrotors unmanned aerial vehicles: A review," *Int. J. Smart Sens. Intell. Syst.*, vol. 9, no. 1, pp. 309–333, Mar. 2016, doi: 10.21307/ijssis-2017-872.

[2] B. J. Emran and H. Najjaran, "A review of quadrotor: An underactuated mechanical system," *Annu. Rev. Control*, vol. 46, pp. 165–180, 2018, doi: 10.1016/j.arcontrol.2018.10.009.

[3] Y. Zhang, Z. Chen, X. Zhang, Q. Sun, and M. Sun, "A novel control scheme for quadrotor UAV based upon active disturbance rejection control," *Aerosp. Sci. Technol.*, vol. 79, pp. 601–609, Aug. 2018, doi: 10.1016/j.ast.2018.06.017.

[4] A. Aboudonia, A. El-Badawy, and R. Rashad, "Active anti-disturbance control of a quadrotor unmanned aerial vehicle using the command-filtering backstepping approach," *Nonlinear Dyn.*, vol. 90, no. 1, pp. 581–597, Oct. 2017, doi: 10.1007/s11071-017-3683-y.

[5] A. A. Najm and I. K. Ibraheem, "Altitude and attitude stabilization of UAV quadrotor system using improved active disturbance rejection control," *Arabian J. Sci. Eng.*, vol. 45, no. 3, pp. 1985–1999, Mar. 2020, doi: 10.1007/s13369-020-04355-3.
[6] W. Dong, G.-Y. Gu, X. Zhu, and H. Ding, "A high-performance flight control approach for quadrotors using a modified active disturbance rejection technique," *Robot. Auto. Syst.*, vol. 83, pp. 177–187, Sep. 2016, doi: 10.1016/j.robot.2016.05.005.
[7] D. Eager, A.-M. Pendrill, and N. Reistad, "Beyond velocity and acceleration: Jerk, snap and higher derivatives," *Eur. J. Phys.*, vol. 37, no. 6, p. 11, 2016, doi: 10.1088/0143-0807/37/6/065008.
[8] M. P. Kelly, "DirCol5i: Trajectory Optimization for Problems With High-Order Derivatives," *J. Dyn. Syst. Meas. Control*, vol. 141, no. 3, p. 15, Mar. 2019, doi: 10.1115/1.4041610.
[9] X. Liang, Y. Fang, N. Sun, and H. Lin, "Dynamics analysis and time-optimal motion planning for unmanned quadrotor transportation systems," *Mechatronics*, vol. 50, pp. 16–29, Apr. 2018, doi: 10.1016/j.mechatronics.2018.01.009.
[10] J. P. Silva, C. De Wagter, and G. de Croon, "Quadrotor thrust vectoring control with time and jerk optimal trajectory planning in constant wind fields," *Unmanned Syst.*, vol. 06, no. 01, pp. 15–37, Jan. 2018, doi: 10.1142/S2301385018500024.
[11] J. R. Hewit and J. S. Burdess, "Fast Dynamic Decoupled Control for Robotics, using Active Force Control," *Mech. Mach. Theory*, vol. 16, no. 5, pp. 535–542, Jan. 1981, doi: 10.1016/0094-114X(81)90025-2.
[12] M. Mailah, "Intelligent active force control of a rigid robot arm using neural network and iterative learning algorithms," Ph.D. dissertation, Dept. Appl. Phys., Electron. Mech. Eng., Univ. Dundee, Dundee, U.K., Aug. 1998. [Online]. Available: https://ethos.bl.uk/OrderDetails.do?uin=uk.bl.ethos.269529
[13] M. Omar, M. Mailah, and S. I. Abdelmaksoud, "Robust active force control of a quadcopter," *J. Mek.*, vol. 40, no. 2, pp. 12–22, Dec. 2017.
[14] X. Ding, X. Wang, Y. Yu, and C. Zha, "Dynamics modeling and trajectory tracking control of a quadrotor unmanned aerial vehicle," *J. Dyn. Syst. Meas. Control*, vol. 139, no. 2, p. 11, Nov. 2017.
[15] A. Alkamachi and E. Erçelebi, "Modelling and genetic algorithm based-PID control of H-shaped racing quadcopter," *Arab. J. Sci. Eng.*, vol. 42, no. 7, pp. 2777–2786, Jul. 2017, doi: 10.1007/s13369-017-2433-2.
[16] A. M. Abdallah, "Flight dynamics nonlinearity assessment across new aerodynamic attitude flight envelope," Ph.D. dissertation, Dept. Aerosp. Eng., Old Dominion Univ., Norfolk, VA, USA, 2015, doi: 10.25777/hakk-hy29.
[17] H. Elkholy, "Dynamic modeling and control of a quadrotor using linear and nonlinear approaches," M.S. thesis, Amer. Univ. Cairo, Cairo, Egypt, 2014. [Online]. Available: http://dar.aucegypt.edu/handle/10526/3965
[18] S.-E.-I. Hasseni and L. Abdou, "Decentralized PID control by using GA optimization applied to a quadrotor," *J. Autom., Mobile Robot. Intell. Syst.*, vol. 12, no. 2, pp. 33–44, Jun. 2018, doi: 10.14313/JAMRIS_2-2018/9.
[19] Z. Mustapa, S. Saat, A. M. Darsono, and H. H. Yusof, "Experimental validation of an altitude control for quadcopter," *ARPN J. Eng. Appl. Sci.*, vol. 11, no. 6, p. 7, Jan. 2016.
[20] Y. Wang, "Quadrotor aircraft design based on the K60 controller," *J. Eng. Sci. Technol. Rev.*, vol. 10, no. 6, pp. 21–30, Dec. 2017, doi: 10.25103/jestr.106.04.
[21] V. Praveen and A. S. Pillai, "Modeling and Simulation of Quadcopter using PID Controller," *Int. J. Control Theory Appl.*, vol. 9, no. 15, pp. 7151–7158, Jan. 2016.
[22] K. Khuwaja, N.-U.-Z. Lighari, I. C. Tarca, and R. C. Tarca, "PID controller tuning optimization with genetic algorithms for a quadcopter," *Recent Innov. Mechtron.*, vol. 5, no. 1, pp. 1–7, Apr. 2018.
[23] J. S. Burdess and J. R. Hewit, "An active method for the control of mechanical systems in the presence of unmeasurable forcing," *Mech. Mach. Theory*, vol. 21, no. 5, pp. 393–400, Jan. 1986, doi: 10.1016/0094-114X(86)90087-X.
[24] S. Arimoto, S. Kawamura, and F. Miyazaki, "Convergence, stability and robustness of learning control schemes for robot manipulators," in *Proc. Int. Symp. Robot Manipulators Recent Trends Robotics, Modeling, Control Edu.*, New York, NY, USA, 1986, pp. 307–316. [Online]. Available: http://dl.acm.org/citation.cfm?id=23592.23632
[25] J.-X. Xu and Y. Tan, *Linear and Nonlinear Iterative Learning Control*. Berlin, Germany: Springer-Verlag, 2003.
[26] J. Dong and B. He, "Novel fuzzy PID-type iterative learning control for quadrotor UAV," *Sensors*, vol. 19, no. 1, p. 24, Dec. 2018, doi: 10.3390/s19010024.
[27] D. Allahverdy, A. Fakharian, and M. B. Menhaj, "Back-stepping integral sliding mode control with iterative learning control algorithm for quadrotor UAVs," *J. Electr. Eng. Technol.*, vol. 14, no. 6, pp. 2539–2547, Nov. 2019, doi: 10.1007/s42835-019-00257-z.
[28] E. Kuantama, T. Vesselenyi, S. Dzitac, and R. Tarca, "PID and fuzzy-PID control model for quadcopter attitude with disturbance parameter," *Int. J. Comput. Commun. Control*, vol. 12, no. 4, pp. 519–532, Jun. 2017, doi: 10.15837/ijccc.2017.4.2962.
[29] D. K. Tiep and Y.-J. Ryoo, "An autonomous control of fuzzy-PD controller for quadcopter," *Int. J. FUZZY Log. Intell. Syst.*, vol. 17, no. 2, pp. 107–113, Jun. 2017, doi: 10.5391/IJFIS.2017.17.2.107.
[30] B. E. Demir, R. Bayir, and F. Duran, "Real-time trajectory tracking of an unmanned aerial vehicle using a self-tuning fuzzy proportional integral derivative controller," *Int. J. Micro Air Vehicles*, vol. 8, no. 4, pp. 252–268, Dec. 2016, doi: 10.1177/1756829316675882.
[31] Z.-Y. Zhao, M. Tomizuka, and S. Isaka, "Fuzzy gain scheduling of PID controllers," *IEEE Trans. Syst., Man, Cybern.*, vol. 23, no. 5, pp. 1392–1398, Sep. 1993, doi: 10.1109/21.260670.
[32] M. Tahmasebi, M. Mailah, M. Gohari, and R. Abd Rahman, "Vibration suppression of sprayer boom structure using active torque control and iterative learning. Part I: Modelling and control via simulation," *J. Vib. Control*, vol. 24, no. 20, pp. 4689–4699, Sep. 2017, doi: 10.1177/1077546317733164.
[33] Z. Zhou, H. Wang, Z. Hu, Y. Wang, and H. Wang, "A multi-time-scale finite time controller for the quadrotor UAVs with uncertainties," *J. Intell. Robotic Syst.*, vol. 94, no. 2, pp. 521–533, May 2019, doi: 10.1007/s10846-018-0837-1.

SHERIF I. ABDELMAKSOUD received the M.S. degree in aerospace engineering from the King Fahd University of Petroleum and Minerals (KFUPM), Saudi Arabia, in 2015. He is currently pursuing the Ph.D. degree with the School of Mechanical Engineering, Universiti Teknologi Malaysia (UTM), Malaysia. His research interests include dynamic systems modeling, active force control, active vibration control, intelligent control systems, and autonomous unmanned aerial vehicles (UAVs).

MUSA MAILAH (Senior Member, IEEE) received the B.Eng. degree in mechanical engineering from Universiti Teknologi Malaysia (UTM), in 1988, and the M.Sc. degree in mechatronics and the Ph.D. degree in robot control and mechatronics from the University of Dundee, U.K., in 1992 and 1998, respectively. He is currently a registered Chartered Engineer (C.Eng.), U.K. He is currently a Professor with the Faculty of Engineering, School of Mechanical Engineering, UTM, and the Head of the Intelligent Control and Automation (iCA) Research Group, UTM. His research interests include intelligent systems, active force control of dynamical systems, robot control, mobile manipulator, applied mechatronics, and industrial automation.

AYMAN M. ABDALLAH received the B.S. and M.S. degrees in aerospace engineering from the King Fahd University of Petroleum and Minerals, Dhahran, Saudi Arabia, and the Ph.D. degree in aerospace engineering from Old Dominion University, Norfolk, VA, USA, in 2015. He is currently an Assistant Professor and the Chairman of the Aerospace Engineering Department, King Fahd University of Petroleum and Minerals. His research interests include new concept for aerodynamic attitude flight envelope, aircraft nonlinearity assessment, and flight dynamics and control.